Green-synthesis of superparamagnetic Fe_3O_4/alginate bio-nanocomposites for heavy metal contamination removal from industrial wastewater

Muharrem Ince
Munzur University: Munzur Universitesi
OLCAY KAPLAN INCE (olcaykaplan@munzur.edu.tr)
Munzur University: Munzur Universitesi https://orcid.org/0000-0002-0709-5546
Burcu Aydogdu
Munzur University: Munzur Universitesi
Hevidar Alp
Munzur University: Munzur Universitesi

Research Article

Keywords: Superparamagnetic, nano-composite material, characterization, experimental design, desirability function, industrial wastewater

Posted Date: March 2nd, 2022

DOI: https://doi.org/10.21203/rs.3.rs-1336564/v1

Abstract

In present study, an efficient superparamagnetic Fe_3O_4/alginate nanocomposite material ($SPFe_3O_4$/alg-NCM) was green-synthesized and used as nanosorbent to remove some heavy metals from industrial wastewater. Green-synthesized $SPFe_3O_4$/alg-NCM was characterized by using fourier transform infrared spectroscopy (FT-IR) with attenuated total reflection (ATR) unit, UV-Vis spectrophotometer, scanning electron microscopy (SEM) with energy dispersive X-ray analysis (EDX), thermogravimetric analysis (TGA) and differential thermal analysis (DTA) techniques. For determination the experimental conditions to ensure maximum adsorption capacity and to find the effects of various variables including initial heavy metal concentration and flow rate on the adsorption efficiency in column system central compoiste design (CCD) was used. To predict of responses and ANOVA a regression model were derived from CCD. The adsorption efficiencies and capacities of $SPFe_3O_4$/alg-NCM were calculated as 31.93 mg g^{-1} for Cd^{2+} and 58.8 mg g^{-1} for Co^{2+}. The obtained results have proven that nanosorbent can be used successfully and effectively to remove metals from industrial wastewaters. In addition, being reusable and inexpensive are other important advantages of nanosorbent.

Introduction

Heavy metals get around to the environment, naturally (erosion of rocks, geological weathering, corrosion of metals, volcanic activities etc.) and anthropogenically especially by the increasing the development of industry (metallurgy, mining operations, fertilizer, paint, and textile industries etc.) (Foroutan et al. 2018; Briffa et al. 2020; Kumar et al. 2021). In addition to being toxic, these metals are not biodegradable and accumulate in the food chain. Heavy metals mixed up in water start with affecting aquatic organisms and affect all living things by passing through the food chain (Foroutan et al. 2018; Kataria and Garg 2018). Investigations about heavy metals are one of the most popular subjects due to the many negative effects on the environment and therefore on humans. It has also led to the development of new methods for heavy metal removal including cadmium and cobalt due to the increasing heavy metal pollution in the environment and water.

Cadmium and cobalt are classified also among the toxic heavy metals by World Health Organization (WHO) and International Programon Chemical Safety (IPCS) that harm the environment (Shafiee et al. 2019). These, like many others, are widely used in many industries. Therefore, they are found as pollutants in wastewater. Limit values for cadmium and cobalt in water have been determined by many international organizations. In drinking water, maximum permissible limits for cadmium is 3 µg L^{-1} for cobalt 1 mg L^{-1} (Zhang et al. 2018; Zharkova and Bobkova 2019).

Cadmium can cause many disorders in human bodies as diarrhea, erythrocyte destruction, skeletal deformity, trichiniasis, renal demage, respiratory problems, skeletal deformity, behavior disorders and cognitive impairment (Kataria and Garg 2018; Shim et al. 2019).

Cobalt is essential for living beings at low concentrations because it is vital cofactor in vitamin B12. In spite of that when it was taken in excess of the required amount it can be causes some injuries in the body (Awual et al. 2020; Chen et al. 2021). Many diseases such as genetic mutations in living cells, inflammations in respiratory tract, nausea and vomit, paralysis, contact allergy, eczema etc., also occur as a result of exposure to cobalt in various ways (Wahlqvist et al. 2020; Awual et al. 2020; Dehghani et al. 2020).

Due to all these negative effects, it is vital to determine and remove all heavy metals such as cobalt and cadmium by effective methods. Although there are many methods, the most preferred method for the separation and determination of elements from past to present is the adsorption method. Among the advantages of the adsorption method, it can be counted that it is economical, effective and easy (Ince et al. 2017; Foroutan et al. 2018). It is also important that many different adsorbents can be used in this method. In literature different low-cost adsorbents, black tea and sage residue (Ziarati et al. 2020), forest biowastes (Pyrzynska 2019), peanut shells (Villar da Gama et al. 2018), greenhouse crop residue (láñez-Rodríguez et al. 2020), bacterial strain *Rhodococcus opacus* and *Rhodococcus rhodochrous* (Dobrowolski et al. 2017), lantana camara (Robert et al. 2018) and mussel shells (Van et al. 2019) were carried out for removing Cd and Co.

Recently, with the development of nanotechnology, nano adsorbents with large surface area, high magnetic properties, high adsorption capacity and easily separable from aqueous solutions, are used in heavy metal removal (Kataria and Garg 2018; Sun et al. 2018).

In this study *Amanita vaginata* mushroom was utilized for obtain Fe_3O_4 superparamagnetic nanoparticles. Than these nanoparticles were coated with alginate that is a natural biopolymer. Since alginate contains a large number of carboxylate groups, it is easy to chelate metal ions (Liu et al. 2020). For this reason, alginate was used as the coating material in the study and it was successfully applied to remove Cd and Co from industrial wastewater samples.

Experimental

Instruments

Characterization was performed FTIR with ATR unit (67000, Japan), TGA-DTA (DTG-60, Shimadzu, Japan), UV-Vis spectrophotometer (UV-Vis1801, Shimadzu, Japan), SEM-EDS (Hitachi SU3500, Japan) and XRD (Rigaku MiniFlex-600, Japan). Devices were utilized of $SPFe_3O_4$/alg-NCM and element loaded $SPFe_3O_4$/alg-NCM. Flame atomic absorption spectrometer (FAAS) (AAnalyst™ 800, PerkinElmer, Inc., Shelton, CT, USA) were used to determine the elements concentrations. Peristaltic pump (Shenchen, Wertheim-Germany) was used to provide solution flow from the column at a certain speed.

Ultrapure water was derived from ultrapure water system (ELGA LabWater/VWS; UK) and a digital pH-meter (EZDO PL-700PV BenchTop, Taiwan) was used pH measurements.

Green-syntesis of $SPFe_3O_4$-NP and preparation process of nanocomposite material ($SPFe_3O_4$/alg-NCM)

The superparamagnetic bio-nanocomposite beads were prepared by a two steps procedure. In the first step $SPFe_3O_4$-NP were synthesized by green-synthesis from the *Amanita vaginata* extract based on Kaplan Ince et al. (2021) method. The obtained $SPFe_3O_4$-NP dried and used in the second step. At the second step, 100 mL of 1% (w/v) alginic acid sodium salt solution was mixed until it became homogeneous under continuous stirring at room temperature for 3 hours. Then, 1 g of $SPFe_3O_4$-NP that obtained in the first step was added and mixed by ultrasonic bath for 1 hour. The homogeneous mixture was added dropwise into 1% (w/v) 300 mL $CaCl_2$ solution with the aid of a pump, causing the rapid creation of spherical beads due to electrostatic interactions between Ca^{2+} ions and guluronate blocks (Kondaveeti et al. 2016). Obtained beads were kept in the $CaCl_2$ solution for 30 minutes after gelation. A plastic sieve was used to remove the beads from the $CaCl_2$ solution and then washed with ultrapure water.

Fixed column preparation and adsorption-desorption studies

Approximately 10 mg $SPFe_3O_4$/alg-NCM were used to stuff the polyethylene columns for solid phase exraction. The column was washed with ultrapure water before passing the solution through the column. Then the experimental conditions pH (1–9 for Cd^{2+} and Co^{2+}), flow rate (4–12 mL min^{-1} for Cd^{2+}, 2–10 mL min^{-1} for Co^{2+}) and initial concentration (10–30 mg L^{-1} for Cd^{2+}, 15–75 mg L^{-1} for Co^{2+}) determined by CCD were applied. Peristaltic pump was used to pass through the solution into the column. The adsorbed Cd^{2+} and Co^{2+} were desorbed by 1 mL 0.1 M of HCl acid and Cd^{2+} and Co^{2+} ions concentrations were determined by using FAAS.

Analytical Method

An experiment process that is ecofriendly, ultra-fast and highly efficient was carried out to remove Cd^{2+} and Co^{2+} ions from various industrial wastewaters. For determination the concentrations of Cd^{2+} and Co^{2+} ions in real samples, a calibration curve was constituted by using standard solutions with known concentrations range from 0.1 mg L^{-1} to 2 mg L^{-1}. For Cd^{2+} ions, while about 10 mg $SPFe_3O_4$/alg-NCM was filled the column and 15 mL of Cd^{2+} solutions pH range from 3 to 7 was adjusted with HCl (0.01–0.1 N) and NaOH (0.01–0.1 N). Solution flow rate (range from 6 mL min^{-1} to 10 mL min^{-1}) and Cd^{2+} ions initial concentrations (15–25 mg L^{-1}) were adjusted and applied to column. For Co^{2+}, about 10 mg $SPFe_3O_4$/alg-NCM was filled the column and 15 mL of Co^{2+} solutions pH (range from 3 to 7) was adjusted using HCl and NaOH reagents. Co^{2+} solution flow rate (range from 4 mL min^{-1} to 8 mL min^{-1}) and Co^{2+} ions initial concentrations (range from 30 mg L^{-1} to 60 mg L^{-1}) were adjusted and applied to column. Both Cd^{2+} ions and Co^{2+} ions solutions were passed the column using a peristaltic pump. After the column loading process, the column filling material ($SPFe_3O_4$/alg-NCM) was desorbed by using 0.1 M HCl (1 mL) and Cd^{2+} ions and Co^{2+} ions were measured using a FAAS. The amount of Cd^{2+} and Co^{2+} adsorbed by the unit mass of $SPFe_3O_4$/alg-NCM were calculated based on following equation (Eq. 1):

$$q = \frac{(Co - Ce)V}{m} \quad (1)$$

where q (mg g^{-1}), C_e and C_0 represent amount adsorbed per gram of $SPFe_3O_4$/alg-NCM, equilibrium concentrations and initial concentration of metal solution (Cd^{2+} and Co^{2+}, mg L^{-1}), respectively. Similarly, m (mg) represents used $SPFe_3O_4$/alg-NCM mass and V (L) refers to the volume of metal solution.

Experimental design for process variables' optimization

To optimize process conditions, the CCD combined with RSM is an effective method. It is useful technique to analyze the independent variables effects on the response along with a collection of statistical data besides mathematical data. Also, CCD technique is provided various estimation and tests such as model underfitting test, regression equation estimation and testing, factors effect test, regression parameters estimation and test along with model determination coefficient calculation. The CCD is known as regression analysis because it is often preferred for estimating parameters as well as establishing relationships between test indexes and continuous variables. Experimental design approach is especially suitable for optimizing complex synergies or antagonistic effects among variables situations (Kaplan Ince and Ince 2019; Ince and Kaplan Ince 2019a, b; Alam et al. 2021). Since it has wide application areas, RSM has been used in many studies (Kaplan Ince et al. 2018; Pala et al. 2019; Serdar et al. 2019).

In this study, to study and optimize the influence of process variables, three-factors with five-levels CCD was selected. To measure the influence of each independent variables including pH (X_1), flow rate (X_2) and initial concentration (X_3) on Cd^{2+} and Co^{2+} adsorption by $SPFe_3O_4$/alg-NCM a CCD

experimental design (Table 1) was chosen. The level of variables was coded as -1, 0 and + 1, respectively. Furthemore, the star points of + 2 and − 2 were defined corresponding to α and -α, respectively, for each set of experiments. The main, interaction and quadratic variables effects are modeled by using CCD. An experimental design based on controllable factors was performed for minimizing the effects of uncontrolled parameters. In addition, optimizing process parameters and monitoring their interactions with a minimum number of experiments is only possible using a design such as a CCD.

Table 1
Experimental parameters for Cd and Co and their levels in the CCD

Run	pH	Flow rate (mL min^{-1})	Cd initial concentration ($mg\ L^{-1}$)	mg Cd/g Ads	Run	pH	Flow rate (mL min^{-1})	Co initial concentration ($mg\ L^{-1}$)	mg Co/g Ads
1	5	8	20	**12.75**	1	3	8	30	**8.35**
2	5	8	20	**9.9**	2	3	4	60	**7.7**
3	5	4	20	**12.9**	3	3	8	60	**22.6**
4	7	10	25	**26.3**	4	5	6	75	**58.8**
5	5	8	20	**11.4**	5	5	6	45	**3.3**
6	9	8	20	**27.3**	6	7	8	60	**44.4**
7	5	12	20	**10.5**	7	7	4	30	**12.3**
8	7	6	15	**13.2**	8	5	6	15	**18.3**
9	1	8	20	**12.7**	9	7	8	30	**9.75**
10	5	8	20	**11.4**	10	5	6	45	**4.5**
11	5	8	20	**10.4**	11	5	6	45	**4.25**
12	5	8	10	**13.4**	12	7	4	60	**40.3**
13	3	10	25	**13.7**	13	5	2	45	**6.3**
14	5	8	20	**11.6**	14	5	6	45	**3.3**
15	7	10	15	**10.2**	15	9	6	45	**34.4**
16	3	10	15	**13.6**	16	5	10	45	**17.1**
17	3	6	25	**14.9**	17	5	6	45	**3.6**
18	3	6	15	**8.4**	18	5	6	45	**4.45**
19	5	8	30	**30.3**	19	3	4	30	**3.1**
20	7	6	25	**32.4**	20	1	6	45	**1.75**

Results And Discussion

Lately in studies nanoparticles whose surfaces were modified and in the way the adsorption capacity was increased are used. For these studies, SPFe_3O_4-NP were coated with iron phosphate (Zhang et al. 2018), Fe_3O_4 nanoparticles were encapsulated into calcium alginate coated chitosan hydrochloride hydrogel beads (Yi et al. 2018), graphene oxide@Fe_3O_4 magnetic beads were compounded with carboxymethyl chitosan and sodium alginate (Wu et al. 2019), Fe_3O_4/layered double hydroxides were trapped into calcium alginate (Sun et al. 2018), Fe_3O_4 nanoparticles were coated with sodium alginate (Serunting et al. 2018), the mixture of titanium oxide and maghemite nanoparticles immersed in polyvinyl alcohol-alginate beads (Majidnia and Idris 2015) can be given.

El-Shamy et al. (2019) used magnetite-alginate nanoparticles for Co ions adsorption from wastewaters. Co ions concentrations were determined by AAS. The adsorption efficiency and absorption capacity were calculated as 95.01% and 33.557 mg g^{-1}, respectively.

In a study bionanocomposite were produced and used for copper and nickel removal. The bionanocomposite adsorption capacity was evaluated 88.49 mg g^{-1} for copper and 86.95 mg g^{-1} for nickel (Foroutan et al. 2018).

Hosseinzadeh et al. (2016) obtained nanocrystalline magnetite from hematite and used for Cd^{2+} removal in aqueous solutions. In order for cadmium not to precipitate as hydroxides, it has not been studied greater than 7 pHs'. It was stated that pH is the most effective parameter among the experimental parameters for metal removal, such as initial concentration, contact time and temperature.

In a batch system, biochar produced from greenhouse crop residue was used as adsorbent for Co removal. For adsorbent activation different materials were applied. The adsoption capacity was calculated as 30.98 mg g^{-1} (láñez-Rodríguez et al. 2020).

Kataria and Garg (2018) synthesized two different iron oxide nanoparticles and used these nanoparticles metal removal from ground water by batch technique. They studies effects of pH, adsorbent dose, temperature, contact time on adsorption and reusability of adsorbents. Adsorption capacities of nanoparticles were found 51 mg g^{-1} and 63.3 mg g^{-1}.

In a study magnetite – manganese oxide nanoparticles immobilized by alginate. Optimum conditions for Cd^{2+} removal were selected 6 for pH, 30°C for temperature, 120 min for contact time and 10 mg for the adsorbent amount (Kumar et al. 2021).

In this study nanoparticles coated with alginate and the adsorbent adsorption capacity found high for Cd^{2+} (31.93 mg g^{-1}) and Co^{2+} (58.8 mg g^{-1}) ions. Because alginate molecules are occurred from carboxyl, carbonyl, and hydroxyl other groups so the obtained nanoparticles can easily adsorb the Cd^{2+} and Co^{2+} (Cheng et al. 2019).

Characterization of $SPFe_3O_4$/alg-NCM

Spectra of the pretreated alginate, $SPFe_3O_4$/alg-NCM and Cd^{2+}/Co^{2+} ions loaded $SPFe_3O_4$/alg-NCM were compared by using FTIR-ATR. FTIR-ATR analyses were used to characterize the changes of functional groups before and after Cd^{2+}/Co^{2+} biosorption. The same characteristic bands were seen in the FTIR spectra (Fig. 1) for the alginate coated beads, $SPFe_3O_4$/alg-NCM and Cd^{2+}/Co^{2+} ions loaded $SPFe_3O_4$/alg-NCM: a wide band between 3400 and 3000 cm^{-1} corresponds to the OH stretch vibration. Weak peaks at 2921, 2936, 2936 and 2923 cm^{-1} in the spectrum of alginate, $SPFe_3O_4$/alg-NCM and $SPFe_3O_4$/alg-NCM loaded with Cd^{2+}/Co^{2+} ions, respectively, and C–H belongs to asymmetric stretching vibration, alginate macromolecule and “egg-box” structures formed by calcium ion limit CH stretching (He et al. 2012). Metal complexes occur in different types; it can coordinate in an ionic or uncoordinated form, via non-identical coordination, via bidentate chelation coordination, and through bicognate bridging coordination. In studies of acetate carboxyl groups, there is a clear relationship between the $v_{asym}(COO^-)$ ve $v_{sym}(COO^-)$ bands of the FTIR spectrum and the metal coordination type, so the separation of bands (i.e. $\Delta v = CO_{asym}\text{-}CO_{sym}$) is also indicative of a specific carboxylate structure. In this study, COO-stretching (asymmetric) spectrum peaks were observed at 1593, 1592, 1601 and 1618 cm^{-1}, respectively. In addition, COO-stretching (symmetrical) spectrum peaks are also seen at 1404, 1416, 1346 and 1345 cm^{-1}. Therefore, $\Delta v(COO^-)_{complex}$ values were found to be 189, 176, 255 and 273, respectively, and $SPFe_3O_4$/alg-NCM is associated with bidentate bridging coordination and $SPFe_3O_4$/alg-NCM loaded with Cd^{2+}/Co^{2+} ions is associated with undefined coordination. Metal–carboxylate interactions in metal–alginate complexes studied with FTIR spectroscopy. Differently, another important band was detected at 541 cm^{-1} which corresponds to the stress vibration of Fe-O bonds in $SPFe_3O_4$-NP of $SPFe_3O_4$/alg-NCM (Huber 2005). In Cd^{2+}/Co^{2+} ions loaded $SPFe_3O_4$/alg-NCM, this peak shift is seen in 561 and 557cm^{-1} and there is no peak in pure alginate.

Thermogravimetric analysis of alginate, $SPFe_3O_4$/alg-NCM and Cd^{2+}/Co^{2+} loaded $SPFe_3O_4$/alg-NCM were recorded in the temperature range of 30°C – 600°C (Fig. 2a). Alginate, $SPFe_3O_4$/alg-NCM, and Cd^{2+}/Co^{2+} ions loaded $SPFe_3O_4$/alg-NCM exhibited similar behavior, showing the formation of magnetic particles in alginate did not change the original structure of alginate and interactions between alginate chains and magnetite or Cd^{2+}/Co^{2+} ions are not strong enough to change their thermal stability. Mass losses in alginate, $SPFe_3O_4$/alg-NCM and Cd^{2+}/ Co^{2+} ions loaded $SPFe_3O_4$/alg-NCM were observed in three stages.

(i) mass losses of 25% from 35°C to 300°C based upon the release of water and CO_2 molecules; (ii) losses from 300°C to 450°C were 80%, 40%, 35% and 39% were attributed to alginate decomposition products, and (iii) losses were 88%, 44%, 44% and 45%, respectively, up to 600°C and decomposition was complete. TGA analyses showed that Cd2+/Co2 + ions loaded SPFe3O4/alg-NCM have a high thermal stability. Also based on TGA-DTA analysis it is very evident that no significant change was observed in the decomposition temperature of $SPFe_3O_4$/alg-NCM and Cd^{2+}/Co^{2+} ions loaded $SPFe_3O_4$/alg-NCM.

The peaks obtained from the DTA plot of alginate, $SPFe_3O_4$/alg NCM and Cd^{2+}/Co^{2+} loaded $SPFe_3O_4$/alg NCM (Fig. 2b) allowed us to obtain more detailed information about thermal degradation. The decomposition of alginate is endothermic, which appears to provide complete degradation at 435°C, and the $SPFe_3O_4$/alg-NCM degradation is exothermic and appears to provide complete degradation at 300°C, which is evidence of the presence of Fe_3O_4 in it. Cd^{2+} loaded $SPFe_3O_4$/alg-NCM degradation is also exothermic and it can be seen from the peaks at 250°C and 315°C, which are determined to be in two stages, in the same way, the degradation of Cd^{2+} loaded $SPFe_3O_4$/alg-NCM is also exothermic, and it is determined to occur in two stages at 250°C and 290°C it can be seen from the peaks at 250°C and 290°C. These results show that Fe_3O_4 is loaded and Cd^{2+}/Co^{2+} were absorbed.

From UV-Vis spectrophotometer analysis it was observed that the color will change from yellow to black immediately when the biomass extract was added to the $FeCl_3$ and $FeCl_2$ solutions and adjust the pH. In addition, the UV-Vis spectra of $SPFe_3O_4$-NP have shown in Fig. 3. In this figure it can be seen a broad absorption around 550 to 750 nm after reaction, indicating the production of $SPFe_3O_4$-NP. Both color change and UV-Vis absorption around 400–580 showed that $SPFe_3O_4$-NPs were successfully synthesized (Huber 2005). Formation of iron oxide nanoparticles is proven with peaks at 298–301 nm (Pattanayak and Nayak 2013).

Samples were analyzed at positions between the angle of 0°-80° 2θ. The 2θ characteristic reflection peaks in the XRD spectrum (Fig. 4) were observed at 29°, 31°, 35°, 38°, 47°, 57° and 62°. From XRD patterns it can be seen sharp peaks. These sharp peaks indicate that the Cd^{2+} and Co^{2+} loaded $SPFe_3O_4$/alg-NCM have high crystallinity structure. Peaks at 35.34°, 35.43° and 35.57° shows us the presence of iron. The most severe peaks were observed to be 29°.

As it can be seen EDS graph in Fig. 5, the amounts of O, Fe, Na are higher than the other elements. The excess of O and Fe is due to Fe_3O_4, and the excess of Na is due to sodium alginate. It is also seen that Cd^{2+} and Co^{2+} are loaded into the $SPFe_3O_4$/alg-NCM.

Shape and size distribution of the nanoparticles were investigated using SEM analysis for distinguishing morphological properties and presented in Fig. 6. SEM visual micrograph of $SPFe_3O_4$/alg-NCM represents the nanoparticles spherical and uniform distribution of on the alginate surface. As can be observed that after interaction by Cd^{2+} and Co^{2+} ions, the nanoparticles still retain their spherical morphology.

RSM statistical analysis and model fitting

The CCD combined with RSM was selected and performed to optimize of crucial variables and explain the response surface nature. Regression coefficients and ANOVA results reveal that quadratic model ($p < 0.0001$) nature very important both for Cd^{2+} and Co^{2+} ions. While Table 2 presents CCD programme, Table 3 presents ANOVA test results that contain suggested second-order equation coefficients and model terms for Cd^{2+} and Co^{2+} ions adsorption on $SPFe_3O_4$/alg-NCM. Suggested model variables were tested using Fisher's test. Because with this test, it shows that larger “F values” and smaller “p values” are more meaningful than the proposed model terms. In this study; while p value of less than 0.05 indicated significance at the 95% confidence level, F value of 95.55 represented that the model is important. The "Probe > F" values are a measure of whether the model terms are statistically significant. If the "Probe > F" value is less than 0.05, it means that the term is statistically significant for the model, and a value greater than 0.05 indicates that that term is statistically insignificant for the model. In this case, both Cd^{2+} and Co^{2+} all model terms including X_1, X_2, X_3, X_1X_2, X_1X_3, X_2X_3, X_1^2, X_2^2 and X_3^2 values are significant model terms (Tables 2 and 3).

Table 2
Analysis of variance (ANOVA) of the Cd^{2+} quadratic model

	Sum of		Mean	F	p-value	
Source	**Squares**	**df**	**Square**	**Value**	**Prob > F**	
Model	997.50	9	110.83	97.03	*< 0.0001*	Significant
X_1-pH	*230.28*	*1*	*230.28*	*201.60*	*< 0.0001*	
X_2-Flow rate	*6.13*	*1*	*6.13*	*5.36*	*< 0.0001*	
X_3-Cd initial concent.	*358.16*	*1*	*358.16*	*313.55*	*< 0.0001*	
X_1 X_2	*21.45*	*1*	*21.45*	*18.78*	*< 0.0001*	
X_1 X_3	*102.96*	*1*	*102.96*	*90.14*	*< 0.0001*	
X_2 X_3	*11.28*	*1*	*11.28*	*9.88*	*< 0.0001*	
X_1^2	*124.47*	*1*	*124.47*	*108.97*	*< 0.0001*	
X_3^2	*0.57*	*1*	*0.57*	*0.50*	*< 0.0001*	
X_3^2	*181.60*	*1*	*181.60*	*158.98*	*< 0.0001*	
Residual	11.42	10	1.14			
Lack of Fit	*6.46*	*5*	*1.29*	*1.30*	*0.3896*	Not significant
Pure Error	*4.96*	*5*	*0.99*			
Cor Total	1008.92	19				
R^2	0.9887					
R^2_{Adj}	0.9785					
R^2_{Pred}	0.9417					
Adeq Precision	30.037					

**p < 0.01 highly significant; 0.01 < p < 0.05 significant; p > 0.05 not significant.*

Table 3
Analysis of variance (ANOVA) of the Co^{2+} quadratic model

Source	Sum of Squares	df	Mean Square	F Value	p-value Prob > F	
Model	5130.88	9	570.10	1476.85	< 0.0001	Significant
X_1-pH	*1061.13*	*1*	*1061.13*	*2748.88*	*< 0.0001*	
X_2-Flow rate	*117.18*	*1*	*117.18*	*303.56*	*< 0.0001*	
X_3-Co initial concentc	*1650.39*	*1*	*1650.39*	*4275.37*	*< 0.0001*	
X_1 X_2	*43.24*	*1*	*43.24*	*112.03*	*< 0.0001*	
X_1 X_3	*239.80*	*1*	*239.80*	*621.22*	*< 0.0001*	
X_2 X_3	*33.21*	*1*	*33.21*	*86.03*	*< 0.0001*	
X_1^2	*324.00*	*1*	*324.00*	*839.34*	*< 0.0001*	
X_3^2	*100.17*	*1*	*100.17*	*259.50*	*< 0.0001*	
X_3^2	*1906.79*	*1*	*1906.79*	*4939.59*	*< 0.0001*	
Residual	3.86	10	0.39			
Lack of Fit	*2.27*	*5*	*0.45*	*1.42*	*0.3548*	Not significant
Pure Error	*1.59*	*5*	*0.32*			
Cor Total	5134.74	19				
R^2	0.9992					
R^2_{Adj}	0.9986					
R^2_{Pred}	0.9963					
Adeq Precision	129.914					

**p < 0.01 highly significant; 0.01 < p < 0.05 significant; p > 0.05 not significant.*

Furthermore, the data variation around the model that fits the experimental data is expressed as the model's lack of fit (LOF). The LOF p-values measure the fitness of the model and imply the LOF is not significant relating to the pure error. The LOF value, which is conclusive evidence for the adequacy of the model fit, provides information about the model fit without the effects of additional higher order terms. Based on Tables 2 and 3 LOF p-values of Cd^{2+} and Co^{2+} are 0.3896 and 0.3548, respectively. These p-values of LOF confirm the suitable applicability for well-fitting of the reaction. Also, the number of experiments performed was found to be sufficient, for determining the independent variables' effects for Cd^{2+} and Co^{2+} ions adsorption on $SPFe_3O_4$/alg-NCM. Polynomial models validity was assessed by determining the determination coefficients (R^2) and determination adjusted coefficients (R^2_{adj}). Because R^2 and R^2_{adj} are defined the percentage of variability in the response. Moreover, it is desirable to have a proposed model high R^2 along with for validity of the model, value of R^2 should be greater than 0.75 (Ince and Kaplan Ince 2017). Obtained R^2 and R^2_{adj} values for the previously mentioned Cd^{2+} and Co^{2+} models were satisfactory. Because R^2 of the models were obtained for Cd^{2+} as 0.9887 for Co^{2+} as 0.9992, it can be said that 98.87% and 99.92% of the model-predicted values matched the experimental adsorbed for Cd^{2+} and Co^{2+} values on $SPFe_3O_4$/alg-NCM. In addition, adequate precision (AP) measures the signal to noise ratio (S/N) and this ratio greater than 4 is desirable. The S/N should be greater than four and it is measure by AP. These values obtained as 30.037 for Cd model and 129.914 for Co model. It can be stated that is indicating an adequate signal both model. In lights of preliminary experiment studies, three critical parameters affecting Cd^{2+} and Co^{2+} adsorption were selected as independent variables. On the other hand, Cd^{2+} and Co^{2+} ions adsorption on $SPFe_3O_4$/alg-NCM (Y) were considered as the dependent variable. In addition, to express the relationship between independent variables and responses, experimental data were fitted to two second-order polynomial mathematical equation (Eqs. 2 and 3) presented as below for Cd^{2+} and Co^{2+}:

$$Y\left(mgCd/gFe_3O_4/algNCM\right) = +45.18 - 7.57X_1 + 3.51X_2 - 4.20X_3 - 0.41X_1X_2 + 0.36X_1X_3 - 0.12X_2X_3 - 0.56X_1^2 + 0.04X_2^2 + 0.11X_3^2$$

2

$$Y\left(mgCo/gFe_3O_4/algNCM\right) = +105.78 - 9.63X_1 - 4.78X_2 - 4.12X_3 - 0.58X_1X_2 + 0.18X_1X_3 + 0.07X_2X_3 + 0.90X_1^2 + 0.50X_2^2 + 0.04X_3^2$$

3

For determining the optimum point and achieving the highest treatment performance the best method is layout of the surface plot in the Cd^{2+} and Co^{2+} ions adsorption on $SPFe_3O_4$/alg-NCM process. The affect of each parameter on Cd^{2+} and Co^{2+} ions adsorption on $SPFe_3O_4$/alg-NCM and their interaction were given in Figs. 7 and 8. Three-dimensional (3D) response surface graphs are useful to determine response maximum, middle and minimum points and they were obtained from quadratic model. Figures 7a and 8a present 3D response surface plots of the influence of pH-flow rate on the adsorption efficiency of Cd^{2+} and Co^{2+} ions on $SPFe_3O_4$/alg-NCM. Both Cd^{2+} and Co^{2+} ions adsorption amount increased when pH increases from 3 to 7 ($p < 0.01$), after which an increase in metal uptake were observed. Although the decrease in the flow rate has a serious effect on the adsorption of Cd^{2+} ions, however, it was observed that Co^{2+} ions adsorption did not show a statistically significant increase or decrease tendency with flow rate change.

A magnetic Fe_3O_4/graphene oxide nanocomposite material was synthzed and used for Pb^{2+} removal from water samples by Thy et al. (2020). The optimum Pb^{2+} ions adsorption onto nanocomposite material conditions were performed by RSM combined with Box-Behnken design approach. In mentioned study, the critical variables such as pH and initial concentration on the adsorption the interactive effects of these parameters were examinated. For determining the model suitability and reliability statistical parameters from quadratic model were analysed using ANOVA. By using the comparison and evaluation with the "p-values" the variables and their interactions effect on the responses were investigated. It was stated that pH "p value" is smaller than 0.0001, thus this factor is highly significant factor for Pb^{2+} removal from water.

On the other hand, it is clear that the amount of adsorbed both Cd^{2+} and Co^{2+} ions were increased when both Cd^{2+} and Co^{2+} ions initial concentration ($p < 0.0001$) were increased (Figs. 7b and 8b). Also, when both Cd^{2+} and Co^{2+} ions solutions' pH increases from 3 to 7 ($p < 0.01$) amount of adsorbed metals were increased. According to ANOVA table, it was confirmed that these two variables had a significant effect on both Cd^{2+} and Co^{2+} ions adsorption. Moreover, it was observed that these two variables interaction was statistically significant ($p < 0.05$).

An investigation was carried out by Rasoulzadeh et al. (2020) for the Pb^{2+} ions adsorption onto Fe_3O_4 nanoparticles and chitosan-coated Fe_3O_4 particles using RSM. According to applied approach model, the optimum conditions were found to be as 0.1 g L^{-1} for Pb (II) concentration, 10.95 for pH and 5.5 mg L^{-1} for adsorbent dosage. Also, maximum removal efficiency of Pb^{2+} ions was calculated as 93.6%. It was reported that Pb^{2+} ions initial concentration directly affects the uptake capacity of the Fe_3O_4 nanoparticles and chitosan-coated Fe_3O_4 particles.

Figures 7c and 8c represents combined effect of flow rate-initial concentration of Cd^{2+} and Co^{2+} ions removal at constant pH. While the adsorption for both Cd^{2+} and Co^{2+} ions increased with the increase in the initial concentration, it was observed that the change of flow rate had a partial effect on the metal adsorption on $SPFe_3O_4$/alg-NCM.

As shown in Figs. 7 and 8, factors including pH and initial concentration were found to be very critical with respect to their centre points. Also, it was used for a combined effect of all the factors on a process besides to analyze variation of the factors. Mentioned factors indicate that Cd^{2+} and Co^{2+} ions removal was highly affected by these variables.

All diagnostic plots for Cd^{2+} and Co^{2+} optimization process by using CCD approach were shown in Fig. 9. For comparing all factors effect on optimum conditions for Cd^{2+} and Co^{2+} ions adsorption on $SPFe_3O_4$/alg-NCM a perturbation plot was carried out (Fig. 10). All parameters especially initial concentrations and pH indicates that Cd^{2+} and Co^{2+} ions removal was highly affected by these variables. Additionally, to check the lambda (λ) value a Box-Cox plot was selected for two metals. For predicting any necessary transformation this plot is often used to enhance the significance of model. No transformation was needed, based on λ values obtained from the plots.

The efficiency of the regression model for both elements and the characteristic charts for evaluation are presented in Fig. 9. Although it is clearly observed that there is a high correlation between the estimated and experimental removal values, the residuals show a normal distribution and this distribution supports the model sufficiently in the real system.

The most important statistical metrics such as lowest p-value and LOF value and along with highest F-value and R^2 were examinated to found maximum desirability function (DF) and select the optimal model. The models desirability values were obtained to be 0.98 and 0.75 for Cd^{2+} and Co^{2+}, respectively (Fig. 11).

The optimum values of the variables used for optimization and the highest desirability values obtained depending on these values are presented in Fig. 12 for both Cd^{2+} and Co^{2+}.

Desorption procedure and $SPFe_3O_4$/alg-NCM reusability studies

Reusability and regeneration, desorption studies were investigated for $SPFe_3O_4$/alg-NCM performans. For this reason, through conducting ten consecutive adsorption-desorption cycles were performed and result were given on Fig. 13. During desorption and reuse process, bio-nano materials can be damaged because of their sensitive structure. For clarifying the adsorption process nature, desorption and reuse studies are useful. In the desorption examination choosing proper eluent is very important. Therefore, various desorption reagents including H_2SO_4, HCl, HNO_3, and CH_3COOH desorption efficiency (Fig. 14) were investigated, and the best desorption eulent was obtained as 0.5 M HCl. Under optimal condition, several experimental studies for reusability were performed using HCl (0.5 M) to test SPFe3O4/alg-NCM, for understanding whether desorption process is damaging. Then, by using the

best efficient eluent (0.5 M HCl) adsorbed elements onto nano-biocomposite separated from the column were desorbed and supernatant's Cd^{2+} and Co^{2+} ions concentration were measured using ETAAS. Regenerated $SPFe_3O_4$/alg-NCM were washed at least five times using ultrapure water to reach neutral pH and it was stored for the next adsorption-desorption cycle. Reusability investigations proved that the SPFe3O4/alg-NCM exhibited excellent renewability and reusability up to at least ten cycles. Furthermore, for Cd^{2+} and Co^{2+} ions removal from industrial wastewater, it has been understood that it has significant potential in practical application. The obtained data are compatible with the data in the literature (Ciesielski et al. 2012; Davodi et al. 2020; Hu et al. 2020; Cheraghipour and Pakshir 2020).

Application to real samples

The developed method was carried out to industrial wastewater samples (IW) at optimum conditions (Table 4). Again, in these conditions standard addition method was applied to real samples. Cd^{2+} and Co^{2+} ion standards of 20 µg L^{-1} and 40 µg L^{-1} were added wastewater samples and the results were given in Table 4. For wastewater samples, contamination factors (CF) were calculated and CF was found in the range of 0.64–1.38 for Cd and 0.36–0.54 for Co. The level of metal pollution is expressed in 4 levels. For low contamination, CF is lower than 1; for moderate contamination, CF is in the range of 1 and 3; for considerable contamination, CF is in the range of and for very high contamination, CF is higher than 6 (Barakat et al. 2019). According to results generally wastewater samples CF is lower than 1.

Table 4
Cd^{2+} and Co^{2+} contents of industrial wastewater

Industrial wastewater (IW)	Cd^{2+} (µg L^{-1})				Co^{2+} (µg L^{-1})		
	SA	Found	Removal (%)	CF	Found	Removal (%)	CF
IW 1	0.0	6.6 ± 0.3		1.32	25 ± 2		0.5
	20	27.1 ± 1.1	100		46 ± 3	100	
	40	47.3 ± 3.2	100		64 ± 4	100	
IW 2	0.0	6.9 ± 0.2		1.38	24 ± 2		0.48
	20	26.5 ± 2.2	99		45 ± 2	100	
	40	47.7 ± 3.1	100		63 ± 3	99	
IW 3	0.0	5.4 ± 0.2		1.08	27 ± 3		0.54
	20	26.4 ± 1.8	100		48 ± 4	100	
	40	45.5 ± 2.0	98		68 ± 3	100	
IW 4	0.0	3.2 ± 0.2		0.64	18 ± 1		0.36
	20	24.4 ± 1.5	100		36 ± 3	98	
	40	43.8 ± 3.3	100		56 ± 2	99	
IW 5	0.0	5.6 ± 0.2		1.12	21 ± 1		0.42
	20	27.0 ± 2.5	100		42 ± 3	100	
	40	46.2 ± 3.6	100		60 ± 5	98	
IW 6	0.0	4.8 ± 0.1		0.96	25 ± 2		0.5
	20	24.9 ± 2.2	100		46 ± 4	100	
	40	43.3 ± 1.9	99		66 ± 4	100	

*SA: Standard Addition

Conclusion

In order to protect the environment, heavy metals, which are one of the most important factors causing pollution, must be removed. For this purpose, in this study, a column system was created to remove Cd^{2+} and Co^{2+} from industrial wastewater samples and a superparamagnetic nanomaterial was obtained from a natural product used as column filler. The obtained supermagnetic nanoparticles were coated with alginate and their characterizations were made using various methods. In order to save many parameters such as the chemical to be used and the time to be spent, the central composite design method has been applied. From the CCD results the parameters, pH and initial element concentrations, have an important effect on adsorption. Superparamagnetic nanoparticles have been used to remove Cd^{2+} and Co^{2+} from wastewater of various factories. The adsorption capacity of $SPFe_3O_4$/alg-NCM for Cd^{2+} and Co^{2+} was calculated as 31.93 mg g^{-1} and 58.8 mg g^{-1}, respectively. It has also been found that the material can be used at least ten times for element removal, which indicates good reusability potential. Its high adsorption potential can be a guide for testing its usage for

removal of other elements. Co^{2+} CF results are lower than Cd^{2+} CF results. For both elements, generally, CF value is found low and water samples low contaminationed with these elements.

A just few samples moderate contaminated with Cd^{2+}.

Declarations

Ethical approval All authors declare that the manuscript has not been published previously.

Consent to participate All authors voluntarily to participate in this research study.

Consent to publish All authors consent to the publication of the manuscript.

Authors Contributions

Muharrem Ince: Supervision, Methodology, Writing- Reviewing and Editing,

Olcay Kaplan Ince: Investigation, Validation, Writing- Original draft preparation.

Burcu Aydogdu: Methodology, Investigation, Writing- Reviewing and Editing.

Hevidar Alp: Formal analysis, Investigation, Writing- Reviewing and Editing.

Funding This study was a part of the project supported by Munzur University Scientific Investigations Project Unit (MUNIBAP- GPMUB021-01).

Competing interests All authors declare that they have no competing interests.

Availability of data and materials All data generated or analyzed during this study are included in this published article.

References

1. Alam E, Feng Q, Yang H et al (2021) Synthesis of magnetic core-shell amino adsorbent by using uniform design and response surface analysis (RSM) and its application for the removal of Cu, Zn, and Pb. Environ Sci Pollut Res 28:1–16. https://doi.org/10.1007/S11356-020-11840-7
2. Awual MR, Hasan MM, Islam A et al (2020) Optimization of an innovative composited material for effective monitoring and removal of cobalt(II) from wastewater. J Mol Liq 298:112035. https://doi.org/10.1016/J.MOLLIQ.2019.112035
3. Barakat A, Ennaji W, Krimissa S, Bouzaid M (2019) Heavy metal contamination and ecological-health risk evaluation in peri-urban wastewater-irrigated soils of Beni-Mellal city (Morocco). Int J Environ Health Res 30:372–387. https://doi.org/10.1080/09603123.2019.1595540
4. Briffa J, Sinagra E, Blundell R (2020) Heavy metal pollution in the environment and their toxicological effects on humans. Heliyon 6:e04691. https://doi.org/10.1016/J.HELIYON.2020.E04691
5. Chen F, Iqbal Khan Z, Zafar A et al (2021) Evaluation of toxicity potential of cobalt in wheat irrigated with wastewater: health risk implications for public. Environ Sci Pollut Res 28:21119–21131. https://doi.org/10.1007/s11356-020-11815-8/Published
6. Cheng Y, Wang K, Tu B et al (2019) High-Temperature Reduction of Calcium Alginate to Carbon Sphere for Efficient Removal of Bivalent Cadmium. ChemistrySelect 4:9058–9064. https://doi.org/10.1002/SLCT.201902329
7. Cheraghipour E, Pakshir M (2020) Process optimization and modeling of Pb(II) ions adsorption on chitosan-conjugated magnetite nano-biocomposite using response surface methodology. Chemosphere 260:127560. https://doi.org/10.1016/j.chemosphere.2020.127560
8. Ciesielski T, Weuve J, Bellinger DC et al (2012) Cadmium exposure and neurodevelopmental outcomes in U.S. children. Environ Health Perspect 120:758–763. https://doi.org/10.1289/ehp.1104152
9. Davodi B, Jahangiri M, Ghorbani M (2020) Particulate Science and Technology An International Journal The lead removal from aqueous solution by magnetic $Fe3O_4$ @polydopamine nanocomposite using Box-Behnken design. Part Sci Technol 38:325–336. https://doi.org/10.1080/02726351.2018.1539796
10. Dehghani MH, Yetilmezsoy K, Salari M et al (2020) Adsorptive removal of cobalt(II) from aqueous solutions using multi-walled carbon nanotubes and γ-alumina as novel adsorbents: Modelling and optimization based on response surface methodology and artificial neural network. J Mol Liq 299:112154. https://doi.org/10.1016/J.MOLLIQ.2019.112154
11. Dobrowolski R, Szcześ A, Czemierska M, Jarosz-Wikołazka A (2017) Studies of cadmium(II), lead(II), nickel(II), cobalt(II) and chromium(VI) sorption on extracellular polymeric substances produced by *Rhodococcus opacus* and *Rhodococcus rhodochrous*. Bioresour Technol 225:113–120. https://doi.org/10.1016/J.BIORTECH.2016.11.040
12. El-Shamy OAA, El-Azabawy RE, El-Azabawy OE (2019) Synthesis and characterization of magnetite-alginate nanoparticles for enhancement of nickel and cobalt ion adsorption from wastewater. J Nanomater 2019:6326012
13. Foroutan R, Esmaeili H, Sanati AM et al (2018) Adsorptive removal of Pb(II), Ni(II), and Cd(II) from aqueous media and leather wastewater using *Padinasanctae-crucis* biomass. Desalin Water Treat 135:236–246. https://doi.org/10.5004/dwt.2018.23179

14. He Y, Zhang N, Gong Q et al (2012) Alginate/graphene oxide fibers with enhanced mechanical strength prepared by wet spinning. Carbohydr Polym 88:1100–1108. https://doi.org/10.1016/J.CARBPOL.2012.01.071
15. Hosseinzadeh M, Seyyed Ebrahimi SA, Raygan S, Masoudpanah SM (2016) Removal of cadmium and lead ions from aqueous solution by nanocrystalline magnetite through mechanochemical activation. J Ultrafine Grained Nanostructured Mater 49:72–79. https://doi.org/10.7508.jufgnsm/2016.02.03
16. Hu X, Hu Y, Xu G et al (2020) Green synthesis of a magnetic β-cyclodextrin polymer for rapid removal of organic micro-pollutants and heavy metals from dyeing wastewater. Environ Res 180:108796. https://doi.org/10.1016/j.envres.2019.108796
17. Huber DL (2005) Synthesis, properties, and applications of iron nanoparticles. Small 1:482–501. https://doi.org/10.1002/SMLL.200500006
18. Iáñez-Rodríguez I, Calero M, Blázquez G et al (2020) Greenhouse Crop residue and its derived biochar: Potential as adsorbent of cobalt from aqueous solutions. Water 12:1282. https://doi.org/10.3390/w12051282
19. Ince M, Kaplan Ince O (2019a) Application of response surface methodological approach to optimize removal of Cr ions from industrial wastewater. At Spectrosc 40:91–97. https://doi.org/10.46770/as.2019.03.003
20. Ince M, Kaplan Ince O (2019b) Heavy metal removal techniques using response surface methodology: Water/wastewater treatment. In: Biochemical Toxicology - Heavy Metals and Nanomaterials. IntechOpen, pp 1–19
21. Ince M, Kaplan Ince O (2017) Box-Behnken design approach for optimizing removal of copper from wastewater using a novel and green adsorbent. At Spectrosc 38:200–207. https://doi.org/10.46770/as.2017.06.005
22. Ince M, Kaplan Ince O, Asam E, Onal A (2017) Using food waste biomass as effective adsorbents in water and wastewater treatment for Cu(II) removal. At Spectrosc 38:142–148
23. Kaplan Ince O, Aydogdu B, Alp H, Ince M (2021) Experimental design approach for ultra-fast nickel removal by novel bio-nanocomposite material. Adv Nano Res 10:77–90. https://doi.org/10.12989/ANR.2021.10.1.077
24. Kaplan Ince O, Ince M (2019) Using Box–Behnken design approach to investigate benzo[a]anthracene formation in smoked cattle meat samples and its' risk assessment. J Food Sci Technol 56:1287–1294. https://doi.org/10.1007/s13197-019-03596-x
25. Kaplan Ince O, Ince M, Onal A (2018) Response surface modeling for Pb(II) removal from alcoholic beverages using natural clay: Process optimization with Box–Behnken experimental design and determination by electrothermal AAS. At Spectrosc 39:242–250. https://doi.org/10.46770/as.2018.06.004
26. Kataria N, Garg VK (2018) Green synthesis of Fe_3O_4 nanoparticles loaded sawdust carbon for cadmium (II) removal from water: Regeneration and mechanism. Chemosphere 208:818–828. https://doi.org/10.1016/J.CHEMOSPHERE.2018.06.022
27. Kondaveeti S, Cornejo DR, Petri DFS (2016) Alginate/magnetite hybrid beads for magnetically stimulated release of dopamine. Colloids Surf B Biointerfaces 138:94–101. https://doi.org/10.1016/J.COLSURFB.2015.11.058
28. Kumar A, Prasad S, Saxena PN et al (2021) Synthesis of an alginate-based Fe_3O_4 – MnO_2 xerogel and ıts application for the concurrent elimination of Cr(VI) and Cd(II) from aqueous solution. 6:3945. https://doi.org/10.1021/acsomega.0c05787
29. Liu Y, Chen J, Liu Z et al (2020) Necklace-like ferroferric oxide (Fe_3O_4) nanoparticle/carbon nanofibril aerogels with enhanced lithium storage by carbonization of ferric alginate. J Colloid Interface Sci 576:119–126. https://doi.org/10.1016/J.JCIS.2020.04.128
30. Majidnia Z, Idris A (2015) Combination of maghemite and titanium oxide nanoparticles in polyvinyl alcohol-alginate encapsulated beads for cadmium ions removal. Korean J Chem Eng 32:1094–1100. https://doi.org/10.1007/S11814-014-0333-7
31. Pala A, Serdar O, Ince M, Onal A (2019) Modeling approach with Box-Behnken design for optimization of Pb bioaccumulation parameters in *Gammarus pulex* (L., 1758). At Spectrosc 40:98–103
32. Pattanayak M, Nayak PL (2013) Green synthesis and characterization of zero valent iron nanoparticles from the leaf extract of *Azadirachta indica* (Neem). World J Nano Sci Technol 2:6–09. https://doi.org/10.5829/idosi.wjnst.2013.2.1.21132
33. Pyrzynska K (2019) Removal of cadmium from wastewaters with low-cost adsorbents. J Environ Chem Eng 7:102795. https://doi.org/10.1016/J.JECE.2018.11.040
34. Rasoulzadeh H, Dehghani MH, Mohammadi AS et al (2020) Parametric modelling of Pb(II) adsorption onto chitosan-coated Fe_3O_4 particles through RSM and DE hybrid evolutionary optimization framework. J Mol Liq 297:111893. https://doi.org/10.1016/j.molliq.2019.111893
35. Robert RJ, Robert RJ, Girish CR (2018) The removal of cobalt, nickel, cadmium and lead from wastewater using *Lantana Camara* as adsorbent. Int J Civ Eng Technol 9:292–303
36. Serdar O, Pala A, Ince M, Onal A (2019) Modelling cadmium bioaccumulation in *Gammarus pulex* by using experimental design approach. Chem Ecol 35:922–936. https://doi.org/10.1080/02757540.2019.1670814
37. Serunting MA, Rusnadi R, Setyorini DA, Ramadan BS (2018) An effective cerium (III) ions removal method using sodium alginate-coated magnetite (Alg-Fe_3O_4) nanoparticles. J Water Supply Res Technol 67:754–765. https://doi.org/10.2166/AQUA.2018.086
38. Shafiee M, Foroutan R, Fouladi K et al (2019) Application of oak powder/Fe_3O_4 magnetic composite in toxic metals removal from aqueous solutions. Adv Powder Technol 30:544–554. https://doi.org/10.1016/J.APT.2018.12.006
39. Shim J, Kumar M, Mukherjee S, Goswami R (2019) Sustainable removal of pernicious arsenic and cadmium by a novel composite of MnO_2 impregnated alginate beads: A cost-effective approach for wastewater treatment. J Environ Manage 234:8–20. https://doi.org/10.1016/J.JENVMAN.2018.12.084

40. Sun J, Chen Y, Yu H et al (2018) Removal of Cu^{2+}, Cd^{2+} and Pb^{2+} from aqueous solutions by magnetic alginate microsphere based on Fe_3O_4/MgAl-layered double hydroxide. J Colloid Interface Sci 532:474–484. https://doi.org/10.1016/J.JCIS.2018.07.132
41. Thy LTM, Cuong PM, Tu TH et al (2020) Fabrication of magnetic iron oxide/graphene oxide nanocomposites for removal of lead ions from water. Chem Eng Trans 78:277–282. https://doi.org/10.3303/CET2078047
42. Van HT, Nguyen LH, Nguyen VD et al (2019) Characteristics and mechanisms of cadmium adsorption onto biogenic aragonite shells-derived biosorbent: Batch and column studies. J Environ Manage 241:535–548. https://doi.org/10.1016/J.JENVMAN.2018.09.079
43. Villar da Gama BM, Elisandra do Nascimento G, Silva Sales DC et al (2018) Mono and binary component adsorption of phenol and cadmium using adsorbent derived from peanut shells. J Clean Prod 201:219–228. https://doi.org/10.1016/J.JCLEPRO.2018.07.291
44. Wahlqvist F, Bryngelsson I-L, Westberg H, Anderssonid L (2020) Dermal and inhalable cobalt exposure-Uptake of cobalt for workers at Swedish hard metal plants. PLoS ONE 15:e0237100. https://doi.org/10.1371/journal.pone.0237100
45. Wu Z, Deng W, Zhou W, Luo J (2019) Novel magnetic polysaccharide/graphene oxide @ Fe_3O_4 gel beads for adsorbing heavy metal ions. Carbohydr Polym 216:119–128. https://doi.org/10.1016/J.CARBPOL.2019.04.020
46. Yi X, He J, Guo Y et al (2018) Encapsulating Fe_3O_4 into calcium alginate coated chitosan hydrochloride hydrogel beads for removal of Cu (II) and U (VI) from aqueous solutions. Ecotoxicol Environ Saf 147:699–707. https://doi.org/10.1016/J.ECOENV.2017.09.036
47. Zhang X, Sun C, Zhang L et al (2018) Adsorption studies of cadmium onto magnetic Fe_3O_4@$FePO_4$ and its preconcentration with detection by electrothermal atomic absorption spectrometry. Talanta 181:352–358. https://doi.org/10.1016/J.TALANTA.2018.01.023
48. Zharkova VV, Bobkova LA (2019) Simultaneous determination of copper(II) and cobalt(II) ions, copper(II) and manganese(II) ions in drinking water using indicator test tubes based on carboxylic cation-exchangers. J Anal Chem 74:527–533. https://doi.org/10.1134/S1061934819050125
49. Ziarati P, Sawicka B, Arabian S (2020) Waste herbal and black tea as a novel adsorbent for detoxification of pharmaceutical effluent. Artic J Med Discov 5:20040. https://doi.org/10.24262/jmd.5.3.20040

Figures

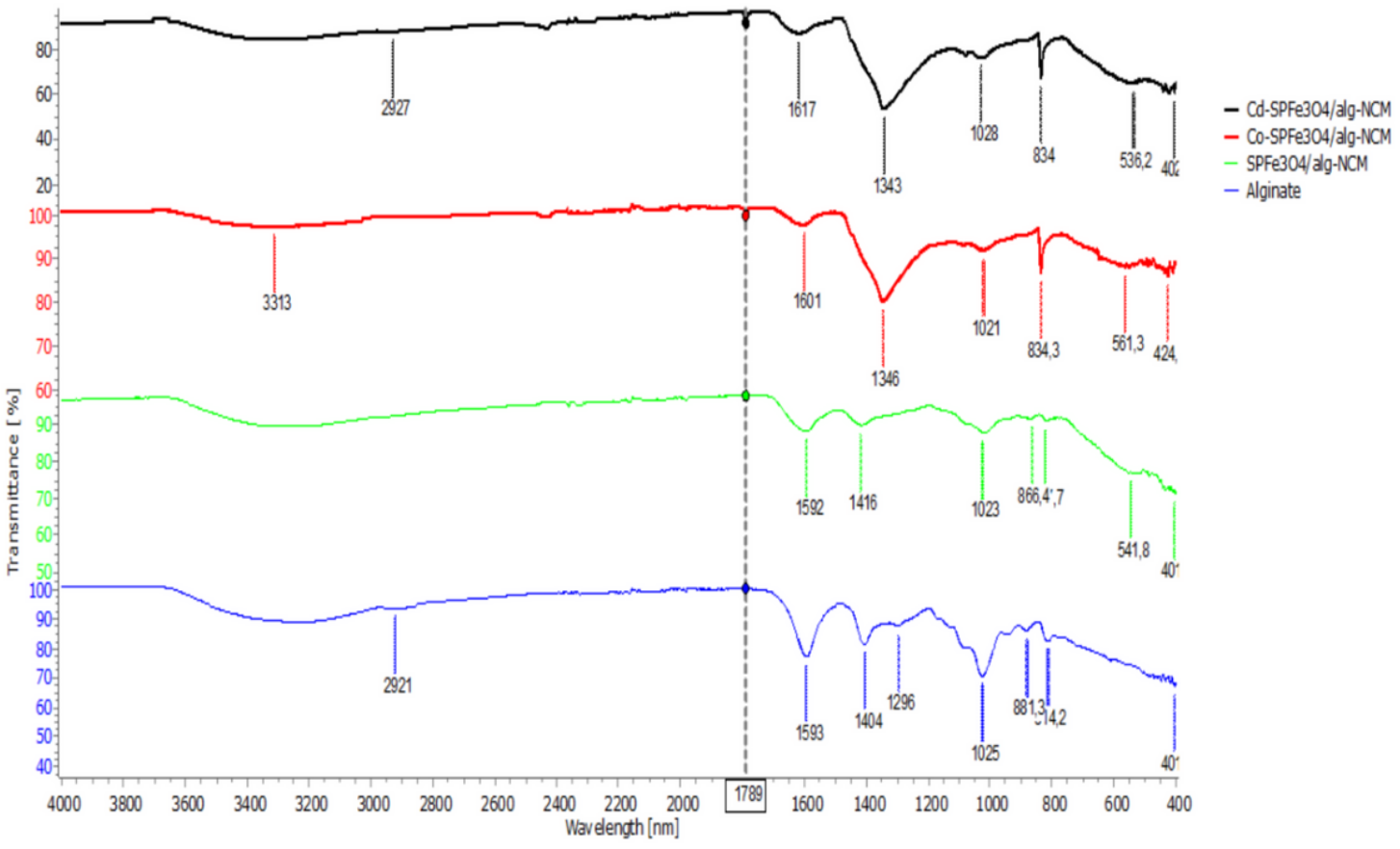

Figure 1

FTIR spectra of $SPFe_3O_4$/alg-NCM and Cd^{2+}/ Co^{2+} ions loaded $SPFe_3O_4$/alg-NCM

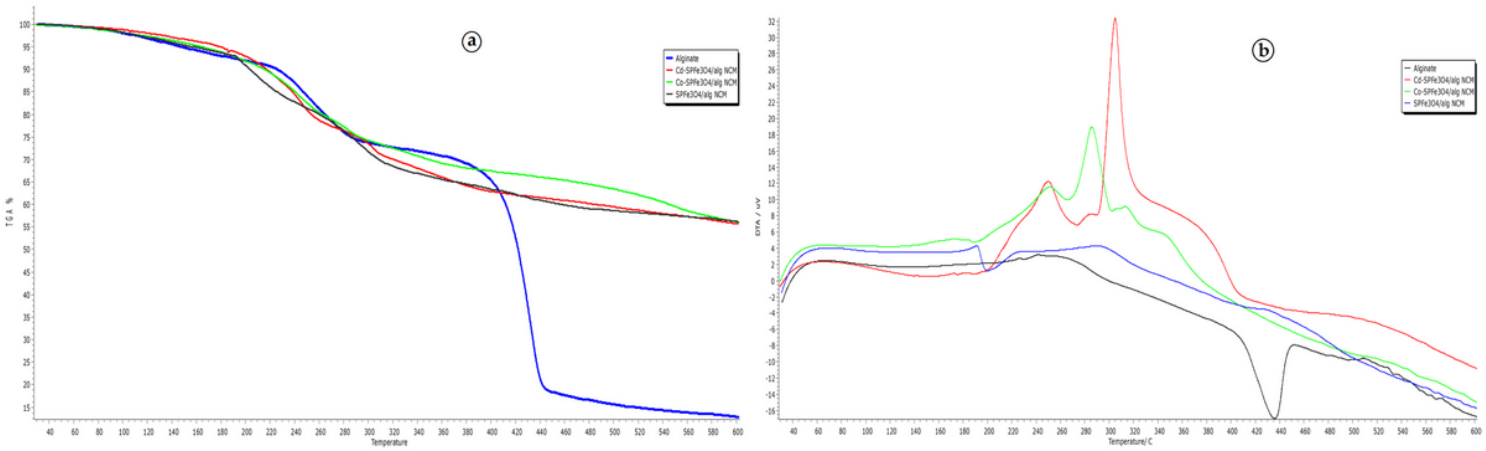

Figure 2

a) TGA and **b)** DTA analaysis of alginate, $SPFe_3O_4$/alg-NCM, Cd^{2+} loaded $SPFe_3O_4$/alg-NCM and, Co^{2+} loaded $SPFe_3O_4$/alg-NCM

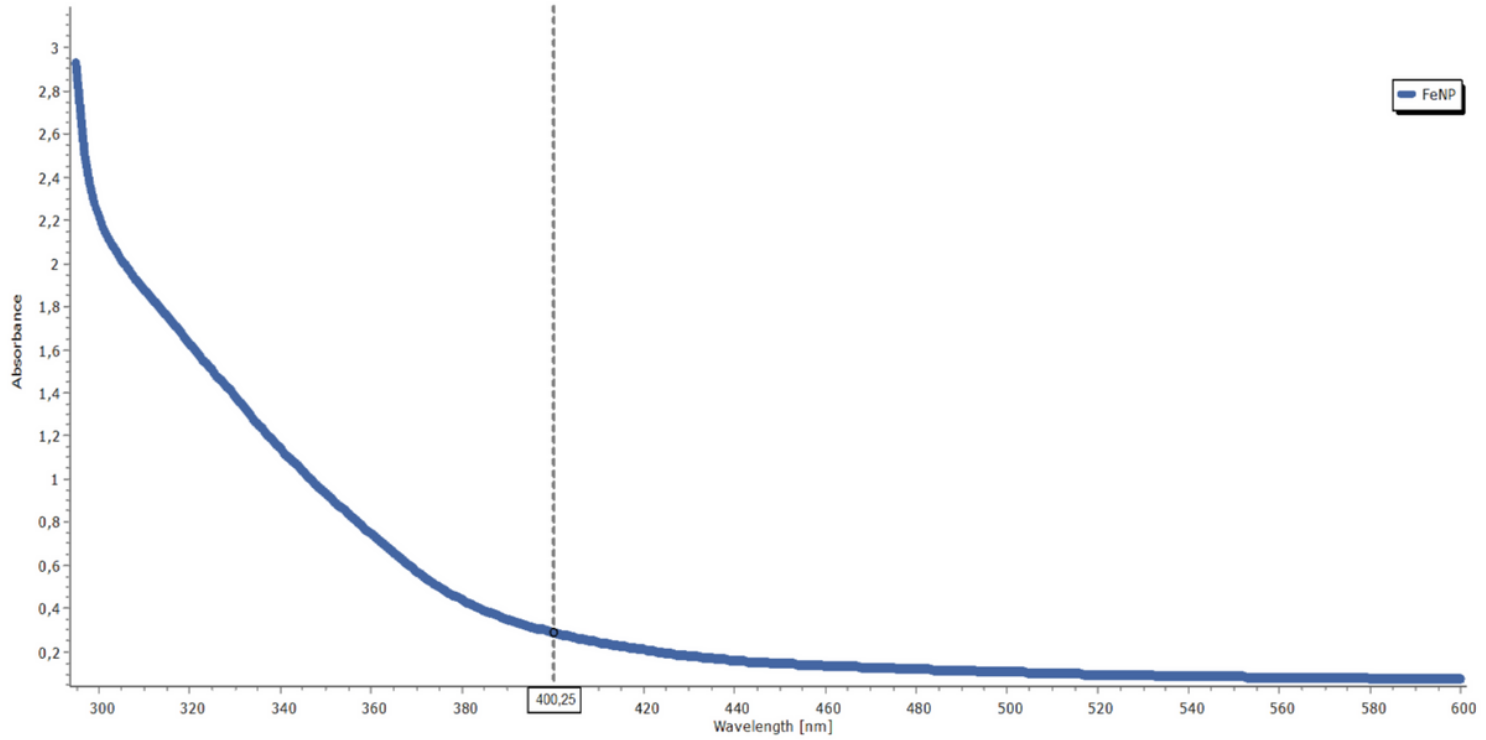

Figure 3

UV-Vis absorption spectra of $SPFe_3O_4$

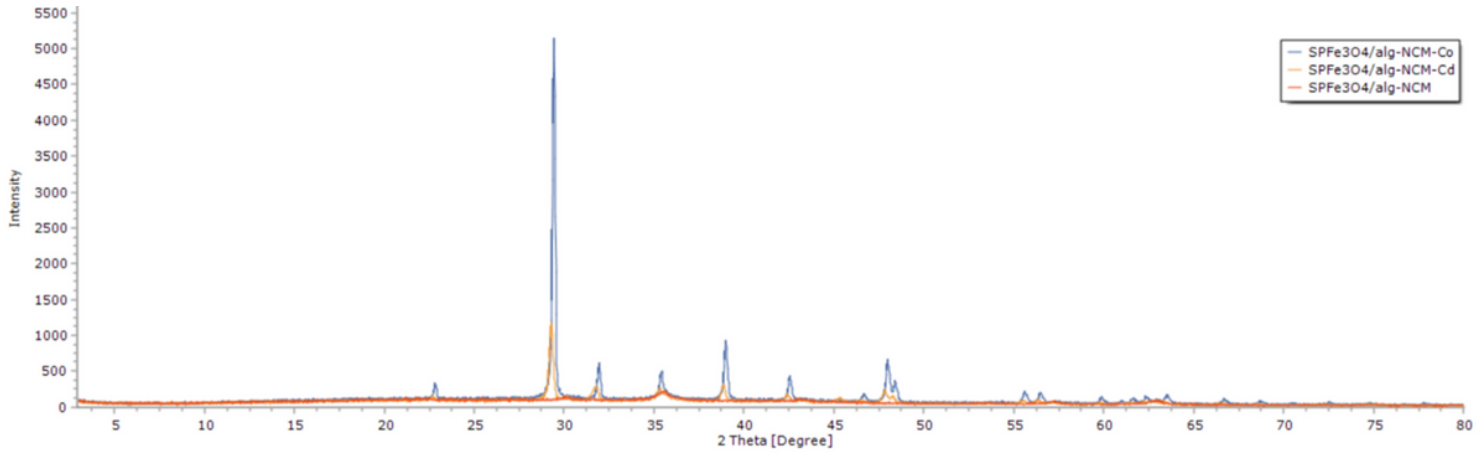

Figure 4

XRD graphs of $SPFe_3O_4$/alg-NCM, Cd^{2+} ions loaded $SPFe_3O_4$/alg-NCM and Co^{2+} ions loaded $SPFe_3O_4$/alg-NCM

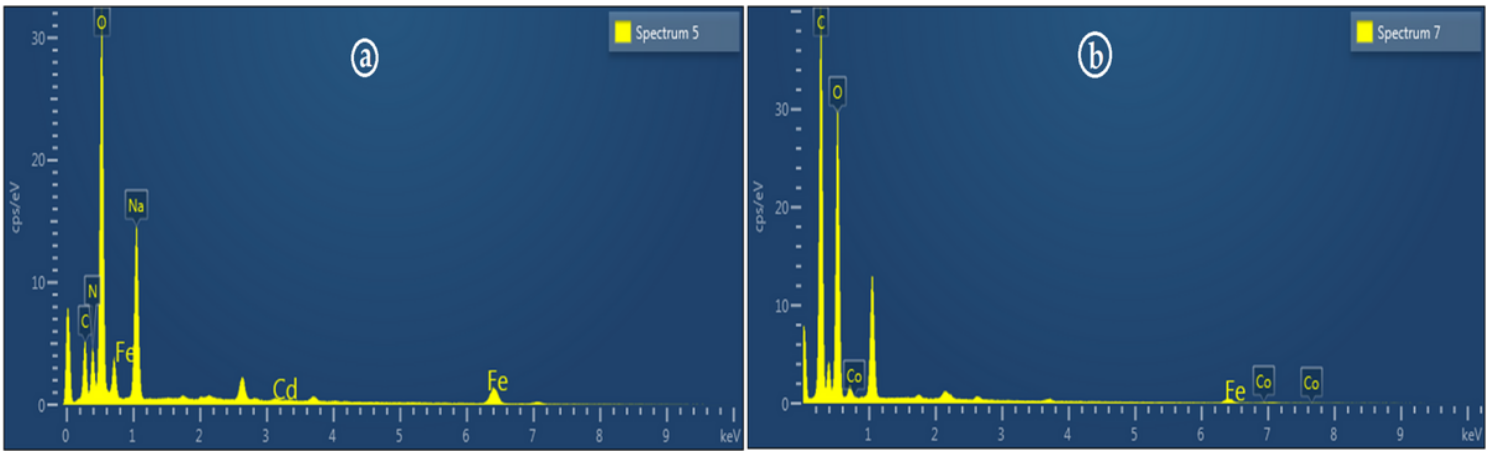

Figure 5

EDS graphs of Cd^{2+} ions loaded $SPFe_3O_4$/alg-NCM and Co^{2+} ions loaded $SPFe_3O_4$/alg-NCM

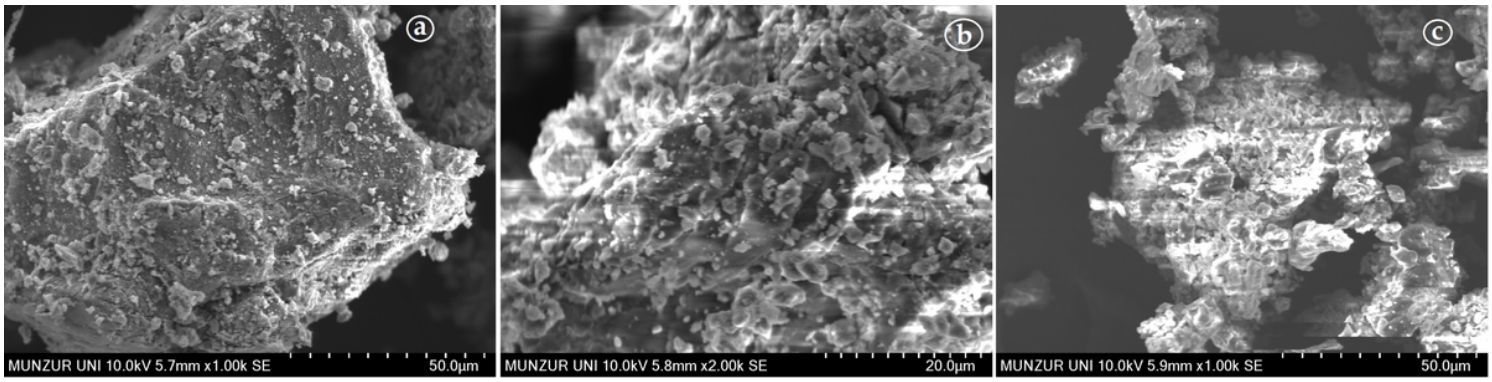

Figure 6

SEM images of Cd^{2+} ions loaded $SPFe_3O_4$/alg-NCM and Co^{2+} ions loaded $SPFe_3O_4$/alg-NCM

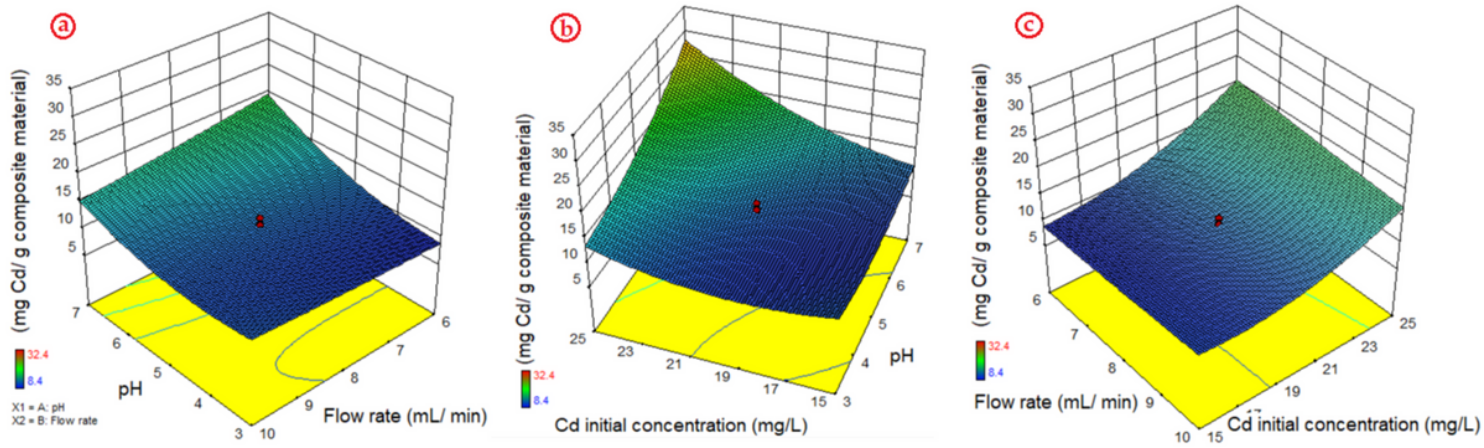

Figure 7

Effect of interaction between a) pH-flow rate, b) pH-initial concentration, c) flow rate-inititial concentration for Cd^{2+}

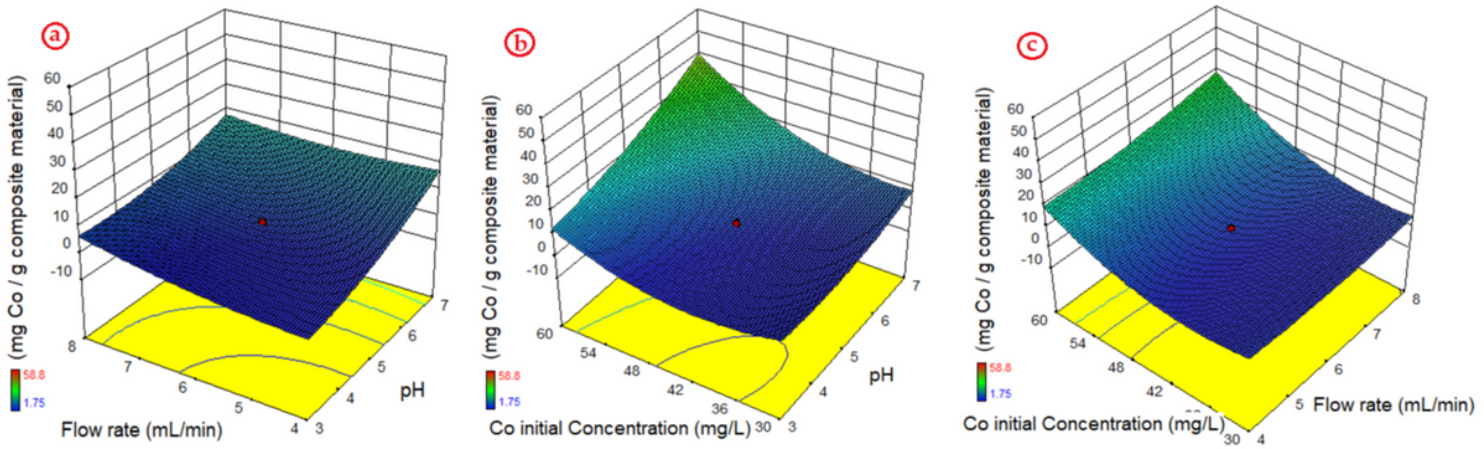

Figure 8

Effect of interaction between a) pH-flow rate, b) pH-initial concentration, c) flow rate-inititial concentration for Co^{2+}

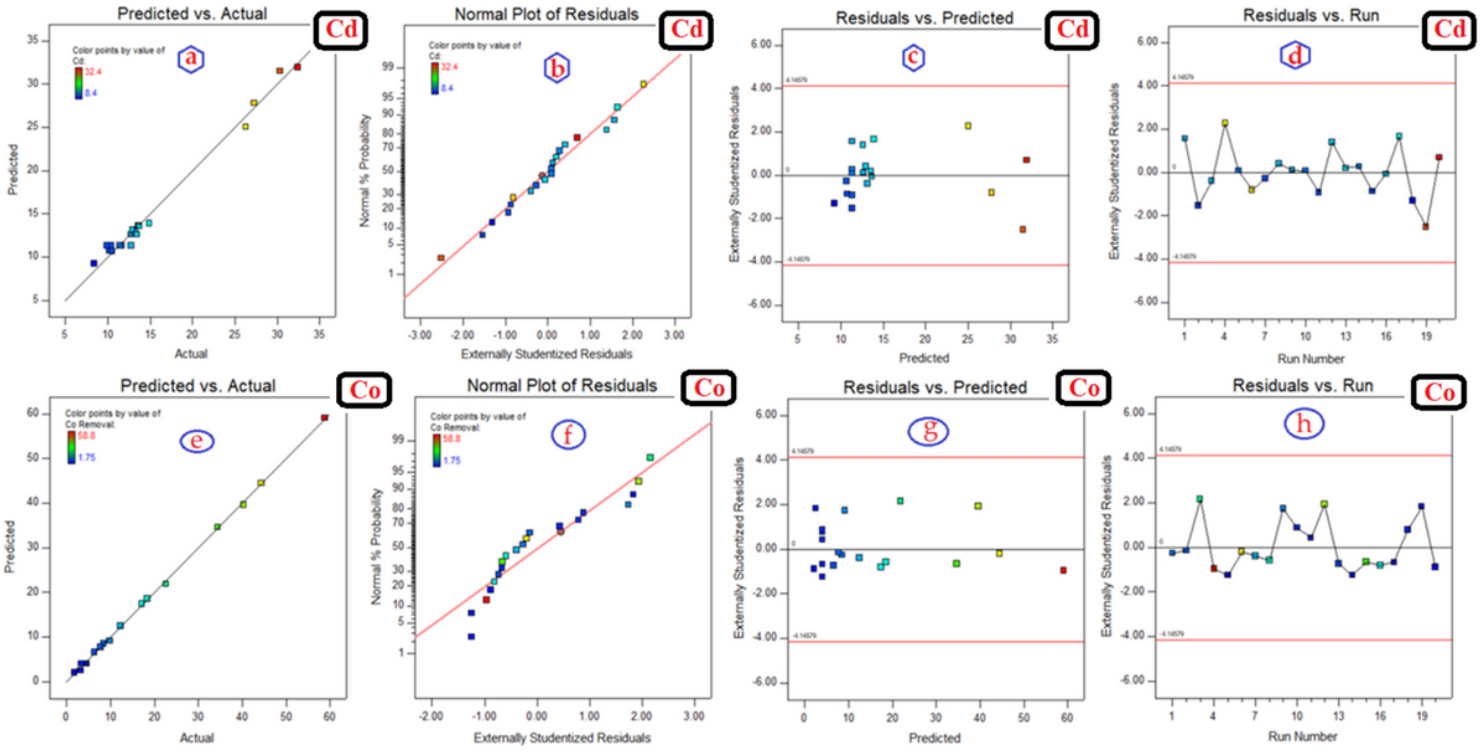

Figure 9

Diagnostic plots: Box-Cox plot and perturbation plot for Cd^{2+} and Co^{2+} removal, at the optimal conditions

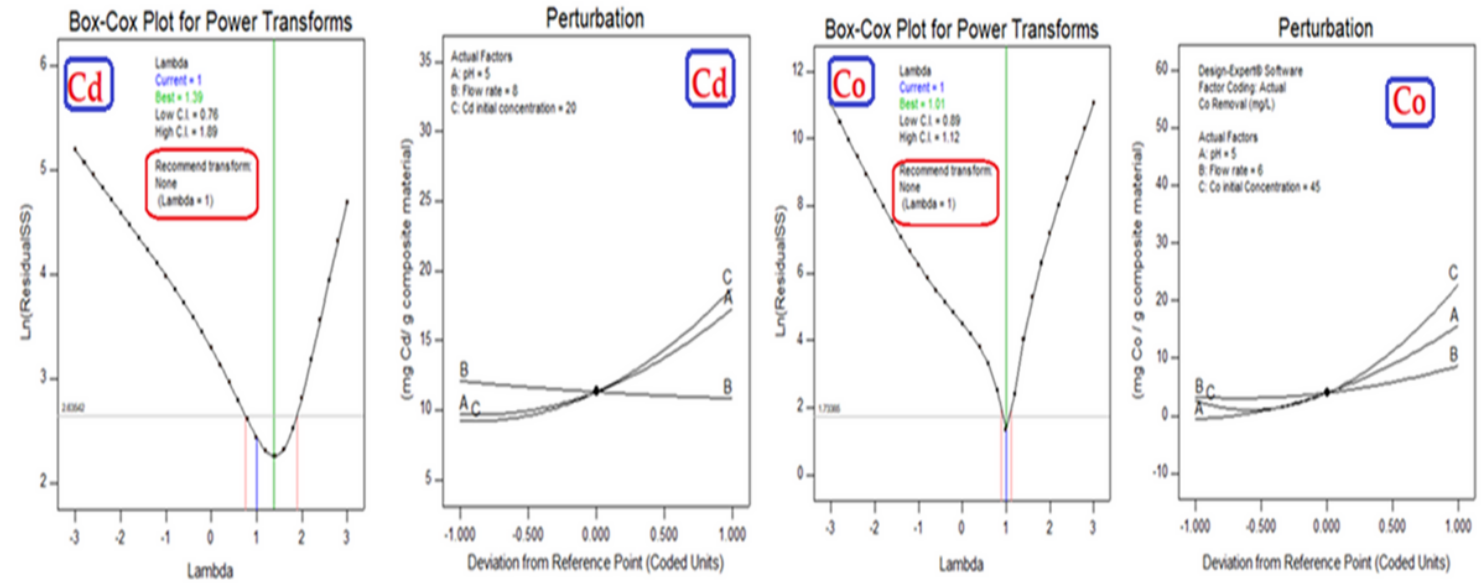

Figure 10

All diagnostic plots of optimization Cd^{2+} and Co^{2+} process using CCD, (a,e) actual and predicted, (b,f) normality, (c,g) studentized residuals and predicted, (d,h) studentized residuals and run values of Cd^{2+} and Co^{2+}

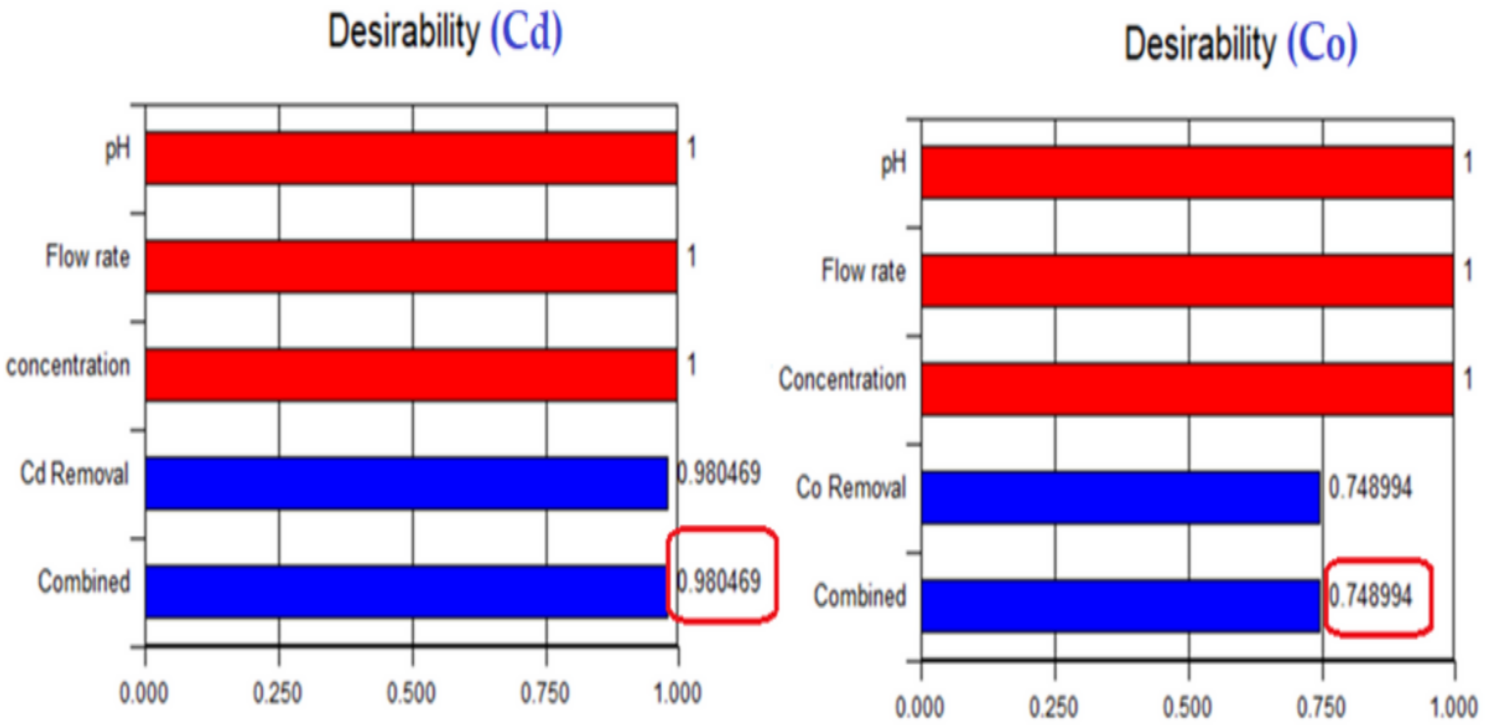

Figure 11

Desirability values for Cd^{2+} and Co^{2+}

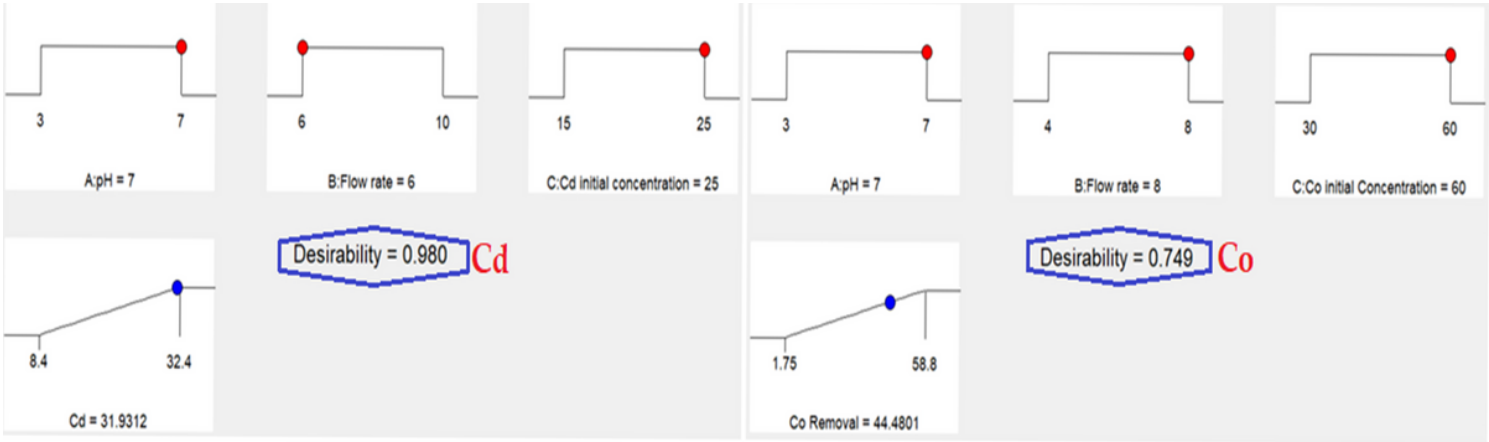

Figure 12

Variables' optimum values and obtained desirability

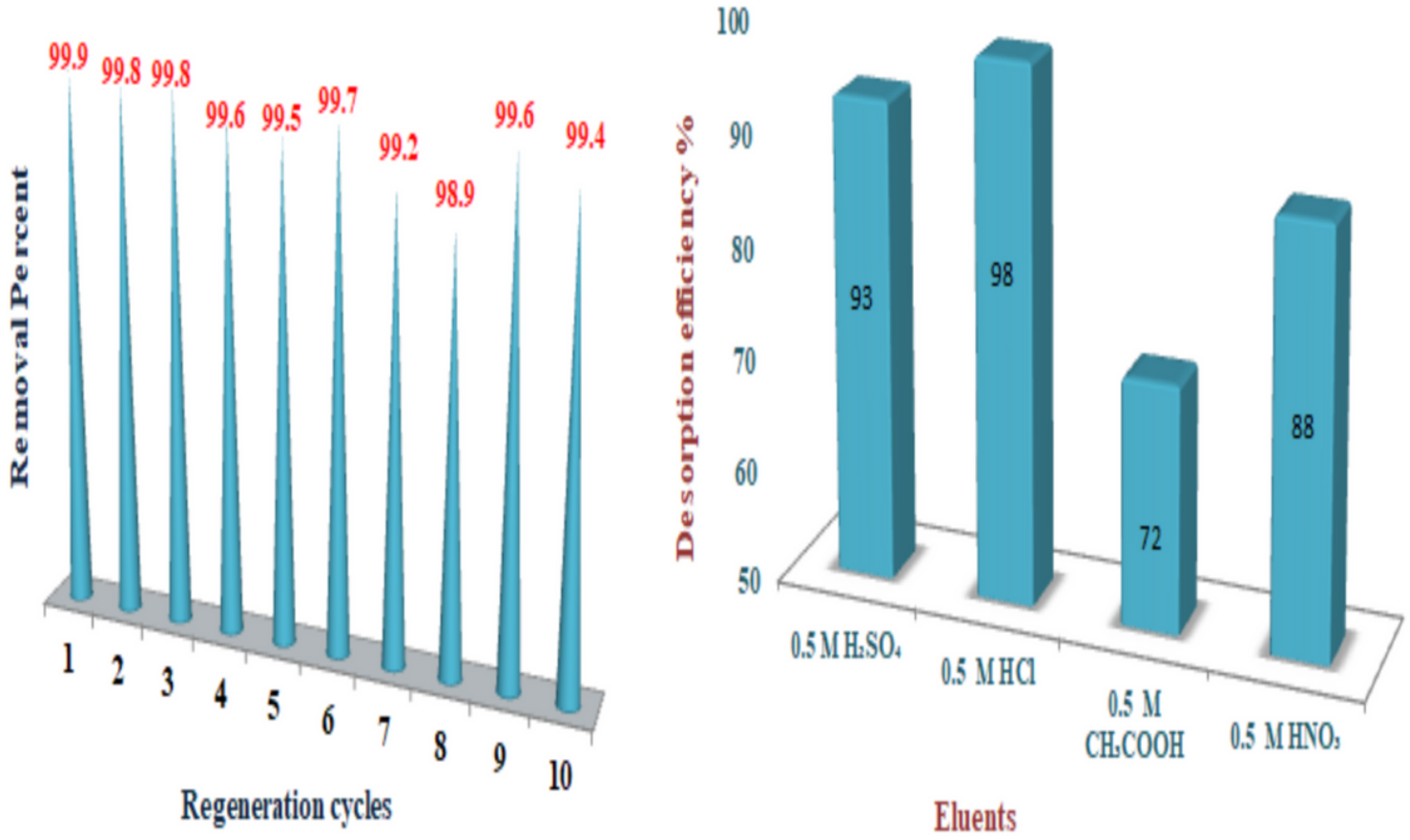

Figure 13

Relative comparison of (a) desorption performance using various eluents and (b) desorption- adsorption of $SPFe_3O_4$/alg-NCM over ten runs in removal of Cd^{2+} and Co^{2+} ions.